Proceedings of the 2025 SICE Festival with Annual Conference
September 9-12, 2025, Chiang Mai, Thailand

Analysis of Rear-Load Bicycle Dynamics for Steering Assist Control

Yuzuki Sugasawa, Keigo Kuriyama, Takaatsu Kihara and Masami Iwase

Department of Robotics and Mechatronics, Tokyo Denki University, Tokyo, Japan
(E-mail: {sugasawa20,kuriyama21,kihara19,iwase}@ctrl.fr.dendai.ac.jp)

Abstract: The objective of this study is to analyze the dynamic behavior of a bicycle under rear-load conditions as a preliminary step toward designing a steering-assist method to improve stability. To this end, a mathematical model of the bicycle is first derived. Simulations using the model are conducted to evaluate the effects of variations in front-wheel geometry and center of mass location on the bicycle's dynamic response. Subsequently, real-world riding experiments are performed using an actual experimental bicycle. The collected data are analyzed to identify unintended behaviors induced by the rear load. As a result, both simulations and experimental results reveal oscillatory behavior in the steering response. These findings confirm that the dynamic characteristics of the bicycle under rear-load conditions have been successfully captured and analyzed.

Keywords: bicycle dynamics, trail effect, rear load, steering oscillation

1. INTRODUCTION

Bicycles are widely used as a means of commuting to work or school, transporting children, and carrying goods, making them a familiar mode of transportation. In Japan, bicycles equipped with child seats on the handlebars or rear carriers-capable of carrying two children-have become common [1]. Furthermore, since riding a bicycle does not require a license, people of all ages and genders use them. In recent years, the spread of shared ride services has made it possible for even those who do not own a bicycle to access one whenever needed [2, 3].

While the demand for bicycles continues to grow, reducing bicycle-related accidents has become a critical issue. Although bicycles are inherently unstable vehicles, stable riding is made possible through the structural design of the bicycle and the rider's ability to maintain balance [4]. The dynamics of bicycles have been extensively analyzed by many researchers [5-7], and various mechanical improvements have been proposed to enhance stability [6]. One example is commercially available electric-assist bicycles, which support acceleration during start-up and assist in uphill riding, allowing users with limited physical strength to maintain stable control even at moderate speeds. However, stability issues remain, particularly at low speeds.

One factor affecting bicycle stability is the change in dynamic behavior when loads are placed in front or rear baskets. Shifts in the center of gravity, changes in load distribution between the front and rear wheels, and increased moments of inertia all influence handling during riding. These changes alter the gravitational torque acting on the frame and the restoring torque generated by the mechanical trail, leading to variations in steering force requirements [8]. Such changes can pose a significant burden for users with limited upper-body strength, such as the elderly or women [1, 9]. As a result, they may experience difficulty in performing emergency maneuvers or maintaining balance, increasing the risk of falling.

Our research group is working on the development of a power steering mechanism to reduce the risk of bicycle falls by assisting the rider's steering input [10]. For example, Kohata et al. developed an experimental bicycle equipped with a power steering mechanism, in which the steering torque is estimated using a disturbance observer, and a corresponding assistive torque is applied to the handlebar to reduce wobbling caused by the load in the front basket [10]. In addition, Kihara et al. proposed a control strategy based on a model that incorporates the roll motion of the bicycle frame, enabling steering-assist control in response to changes in the roll angle [11].

While these studies primarily focus on the effects and control of front-wheel loading, the influence of rear-wheel loading has not been sufficiently investigated. The behavior of a bicycle can change significantly due to loading on the rear carrier and shifts in front-rear load balance [5, 12]. Sato et al. are among the few researchers who have analyzed the dynamics under rear-wheel loading. Through stability analysis based on a bicycle model, they demonstrated how variations in the mass of the loaded carried items affect stability. However, these findings have yet to be experimentally validated, and quantitative empirical verification is still required.

Therefore, the aim of this study is to experimentally analyze the stability of a bicycle under rear-wheel loading conditions. First, a nonlinear mathematical model is derived to accurately reproduce the motion around the steering axis. Next, behavioral changes induced by variations in rear load are reproduced through simulations based on the model, and the results are compared with those reported by Sato et al. Finally, using an experimental bicycle with adjustable trail effect, the effects of loading or not loading items on the rear carrier is analyzed based on measured data.

2. BICYCLE MODEL DERIVATION

In this study, a mathematical model of the bicycle is derived with reference to the model proposed by Karl J. Åström et al. [13]. The bicycle configuration is shown in

† Yuzuki Sugasawa is the presenter of this paper.

Fig. 1, and the corresponding model parameters are listed in Table 1.

This model consists of four rigid bodies: the rear wheel, front wheel, rear frame, and steering assembly. Each rigid body is assumed to be symmetric with respect to the frontal plane of the bicycle. The front and rear wheels are in point contact with the ground, and the forward velocity is assumed to be constant.

To accurately reproduce the dynamics around the steering axis, the model incorporates the trail effect, which is one of the key mechanisms linking the roll angle of the bicycle frame to the steering angle. It also includes tire forces, such as lateral force due to sideslip and camber thrust generated by the roll angle. For the derivation of the equations of motion, the state vector q is defined as $q = \begin{bmatrix} \dot{\phi} & \dot{\theta} & \phi & \theta & \psi \end{bmatrix}^T$.

2.1. Change in the Front Wheel Contact Point

When the bicycle leans in the roll direction, the front wheel rotates accordingly, causing the contact point with the ground is also shifted. Let this shift be represented by δL_3, and the distance to the new contact point be denoted by $\delta L_3'$, as illustrated in Fig. 2. From the geometric relationship shown in Fig. 2, the change in the contact point can be obtained as follows:

$$\delta L_3 = r_f \sin\phi. \tag{1}$$

Therefore, the trail after the change can be expressed as

$$L_3' = L_3 \cos\phi + r_f \sin\phi \cdot \operatorname{sign}\theta. \tag{2}$$

2.2. Lateral Force

In this section, the slip angle and the resulting lateral force are derived. A schematic diagram of the bicycle model undergoing lateral slip is shown in Fig. 3. Only

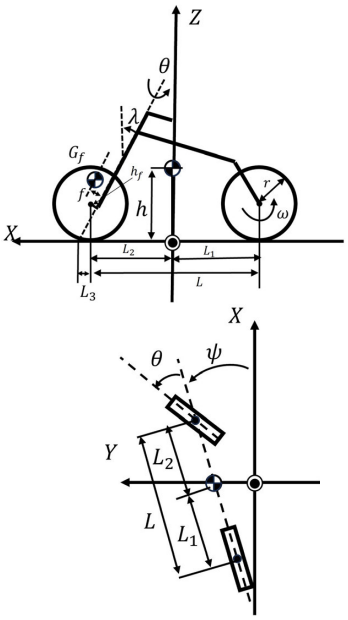

Fig. 1 Bicycle model

Table 1 The independent variable

symbol	description
M	Mass of bicycle
m_f	Mass of front wheel
L	Wheel base
L_1	CoG position from rear wheel contact point
L_2	CoG position from front wheel contact point
L_3	Trail
h	CoG height
f	Fork offset
r_f	Front Wheel radius
r_r	Rear Wheel radius
λ	Caster angle
I_{xx}	Inertia of bicycle body about x axis
I_{zz}	Inertia of bicycle body about z axis
I_{xz}	Inertia of bicycle body about xz axis
I_h	Inertia of steering part
I_f	Inertia of front wheel part
I_r	Inertia of rear wheel part
ϕ	Roll angle
θ	steering angle
ψ	Yaw angle of bicycle body
V	Velocity of bicycle
τ_h	input torque
c	viscous friction
d	coulomb friction
β	Slip angle
C_θ	Cornering stiffness
C_ϕ	Camber stiffness
F_z	Normal load

the lateral slip of the front wheel is considered here. Let the yaw rate be denoted by $\dot{\psi}$ [rad/s], and the turning radius of the rear wheel be b_r [m]. Then, the yaw rate $\dot{\psi}$ can be expressed as

$$\dot{\psi} = \frac{V}{b_r} = \frac{\tan(\theta - \beta)}{L} V. \tag{3}$$

By solving (3) for β, the slip angle can be calculated. The derived expression for the slip angle is given in

$$\beta = \theta - \tan^{-1}\left(\frac{\dot{\psi} \cdot L}{V}\right). \tag{4}$$

The lateral force F_θ generated by sideslip can be expressed as (5), assuming the slip angle β is small as well as [14]

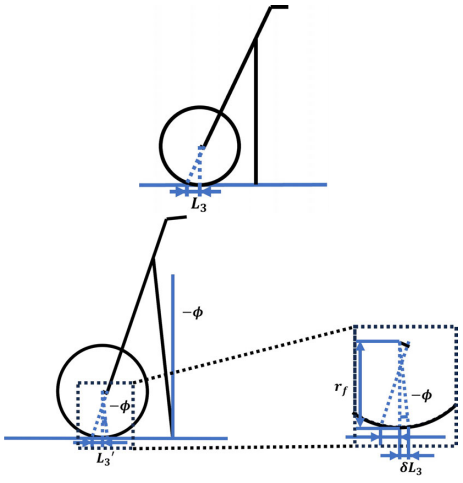

Fig. 2 change in the front wheel contact point

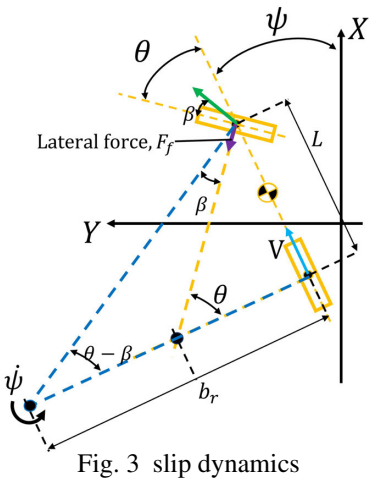

Fig. 3 slip dynamics

$$F_\theta = C_\theta \cdot \beta \cdot F_z. \tag{5}$$

In this section, the camber thrust generated by the inclination of the front wheel is derived. Based on the roll angle, steering angle, and caster angle of the bicycle, the inclination angle of the front wheel can be expressed as $\phi + \theta \sin\lambda$. Using this expression, the camber thrust F_ϕ is given by

$$F_\phi = C_\phi \cdot (\phi + \theta \sin\lambda) \cdot F_z. \tag{6}$$

Considering (2), (5), and (6), the equations of motion for the entire bicycle system are given by (7)–(9)

$$I_{zz}\ddot{\psi} = \frac{L \cdot F_z}{I_{zz}} C_\theta \cdot \beta - C_\phi \cdot (\phi + \theta \sin\lambda) \tag{7}$$

$$\begin{aligned} I_{xx}\ddot{\phi} =& I_{xz}\dot{\theta}\frac{V}{L(\cos^2\theta)} + Mgh\sin\phi + I_r(\dot{\psi})\frac{V}{r_r} \\ &+ Mh\frac{V^2\tan(\theta-\beta)}{(L_1+L_2)} \\ &+ I_f \sec\theta \frac{V}{r_f}(\dot{\psi}+\dot{\theta}) \\ &- Mg\frac{L_1\sin\theta}{L_1+L_2}(L_3\cos\phi + r_f\sin\phi\cdot\mathrm{sign}\,\theta) \end{aligned} \tag{8}$$

$$\begin{aligned} (I_h + I_{xx} + m_f L_3^2)\ddot{\theta} =& -m_f g \sin(\phi - \theta\sin\lambda) f \\ &- I_f \cos\lambda\dot{\phi}\frac{V\tan\theta}{L_1+L_2} + \tau_h - (c\dot{\theta} + d\,\mathrm{sign}\,\dot{\theta}) \\ -(L_3\cos\phi + r_f\sin\phi\cdot\mathrm{sign}\,\theta)&\mathrm{F_z}\sin(\phi-\theta\sin\lambda) \\ &- C_\theta\beta F_z(L_3\cos\phi + r_f\sin\phi) \\ &+ C_\phi(\phi - \theta\sin\lambda)F_z\cos\phi. \end{aligned} \tag{9}$$

3. SIMULATION

Using the equations of motion derived in Section 2, we simulate the bicycle's behavior under variations in the position of the center of gravity.

3.1. Simulation Conditions

The initial values used in the simulation are listed in Table 2. The forward velocity is fixed at 8.0 km/h. To emulate human operation, a control law is implemented that steers the handlebar based on the roll angle and roll rate.

In the simulations, the trail length L_3 and the horizontal distance from the rear wheel contact point to the center of gravity are each varied across three levels, resulting in a total of nine simulation conditions. Table 3 summarizes the parameter settings for each condition.

3.2. Results

The simulation results under fixed trail lengths and varying center of gravity positions are shown in Fig. 4. From top to bottom, the figure presents results for trail lengths of 0.13 m, 0.085 m, and -0.035 m. For each trail length, the curves are color-coded as blue, red, and yellow, representing progressively rearward positions of the center of gravity.

For the trail lengths of 0.13 m and 0.085 m, the amplitude of the steering angle decreased as the center of gravity shifted rearward: from 3 deg to 2 deg, and from 1 deg to 0.5 deg, respectively. In both cases, oscillations containing high-frequency components were observed. In

Table 2 Initial value

state	value
$\dot{\phi}$	0 rad/s
$\dot{\theta}$	0 rad/s
ϕ	-5 deg
θ	1 deg
ψ	2 rad/s

Table 3 Parameter setting combinations

	COG 0.68 m	COG 0.52 m	COG 0.37 m
Trail 0.130 m	Case 1	Case 2	Case 3
Trail 0.085 m	Case 4	Case 5	Case 6
Trail –0.035 m	Case 7	Case 8	Case 9

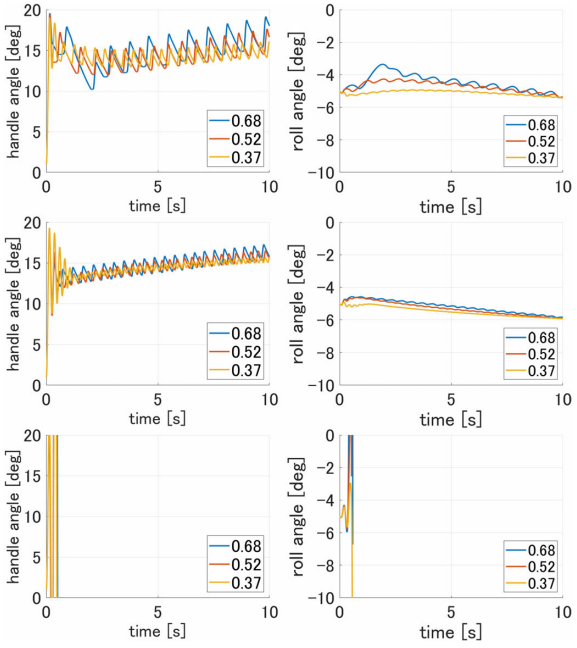

Fig. 4 Simulation results

contrast, for the trail length of -0.035 m, violent steering oscillations occurred within the first 0.7 seconds. The simulation was forcibly terminated when the steering angle reached an absolute value of 90 degrees, indicating instability and breakdown of the system.

4. BICYCLE RUNNING EXPERIMENT

To experimentally validate the findings obtained from the simulations in Section 3, a real-world riding test was conducted using a physical bicycle.

4.1. Experimental Setup

The system configuration diagram of the bicycle used in this study is shown in Fig. 5, and the geometry of each part is presented in Table 4.

This bicycle is equipped with a 3-axis IMU (Inertial Measurement Unit) mounted under the seat, which is capable of measuring angular velocities and angles. In this study, the MEMS IMU model AU7648N from Tama Seiki Co. is used, which can measure 3-axis angular velocities in the range of -200 to 200 deg/s. Additionally, the roll angle and heading angle of the bicycle can be measured in the range of -180 to 180 degrees, and the pitch angle can be measured in the range of -90 to 90 degrees. The sensor has a resolution of 16 bits, and the data sampling frequency is 200 Hz.

Magnets are placed at 4-degree intervals on the rear wheel rim, and changes in magnetic flux are detected using a Hall sensor to calculate the wheel speed. An encoder is mounted on the handlebar to measure the steering angle. Additionally, a motor mounted in the rear wheel is used to control the rear-wheel driving torque to help maintain a constant speed during riding.

The bicycle used in this study allows the trail length to be adjusted by changing the front wheel offset. Fig. 6 shows the condition of the front wheel when the offset is changed. The wheel's fixed point along the extension line of the front fork is set as offset 0, with the direction of motion defined as positive. The offset can be set

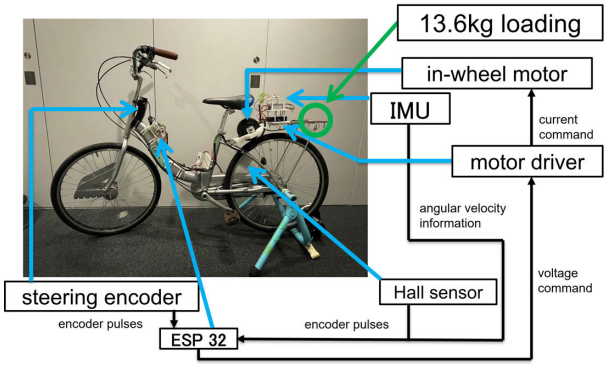

Fig. 5 Bicycle system

Table 4 geometry parameters

Mass	17.5 kg
wheel radius	0.308 m
wheelbase (Trail:0.11m)	1.015 m
caster angle	20.0 deg
horizontal distance from rear wheel to center of mass	0.507 m
steering moment of inertia	0.00181 kgm^2

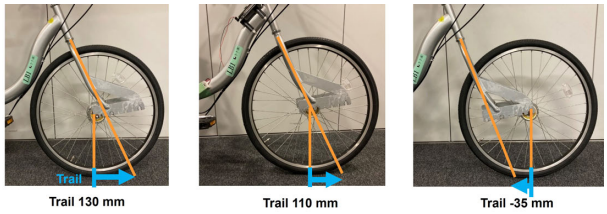

Fig. 6 Variable trail mechanism

in 7 stages: one in the negative direction and five in the positive direction. The distances from each stage and the offset 0 are shown in Table 5.

As shown in Table 5, by varying the offset from -1 stage to +5 stages, the trail length changes from 0.13 m to -0.035 m. In this experiment, the trail lengths are set to 0.13 m, 0.085 m, and -0.035 m, which are the same as those used in the simulation. The experimental environment is shown in Fig. 7.

The experimental surface is a flat asphalt road with a width of 8.0 m and a length of 24.0 m. As shown in Fig. 7, cone markers were placed to define the driving route. To analyze the effect of rear items loading on bicycle behavior during both straight-line and turning motion, a slalom course was adopted as the driving route. The distance between adjacent cone markers was set to 1 meter, and each participant was instructed to follow the same route.

The experiment was conducted using three members of our research group as participants. Their height and weight are listed in Table 6. The riding data obtained in this experiment were collected anonymously and non-invasively, with the goal of developing steering control technology for bicycles loaded with rear items.

This study was conducted in accordance with the guidelines of our university and was deemed exempt from ethical review in this configuration. Participants were ourselves and fully understood the experimental procedures with consent prior to participation. Appropriate measures were also taken to ensure safety and the right to withdraw at any time.

4.2. Experimental Results

In the simulation results of Section 3, a tendency for the steering angle to oscillate at high frequencies was ob-

Table 5 Adjustable trail amount

step	-1	0
Trail [m]	0.13	0.11

step	+1	+2	+3	+4	+5
Trail [m]	0.085	0.055	0.025	-0.05	-0.035

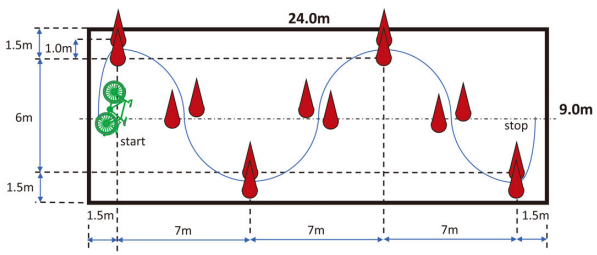

Fig. 7 Experimental setup

Table 6 Participant profiles

Participant	Height [m]	Weight [kg]
First participant	1.78	82.0
Second participant	1.68	53.0
Third participant	1.78	75.0

served when the center of gravity shifted rearward, that is, when cargo was loaded onto the rear carrier. To evaluate this tendency, a frequency analysis of the steering angle was conducted.

However, the measured steering angle includes the steering input required to follow the instructed route. The steering angle needed to perform a slalom maneuver depends on the road curvature and is classified as a low-frequency component in the steering data. The residual (middle to high-frequency components) obtained by removing the low-frequency component reflects the behavior that the rider unconsciously or reactively controls. This study focuses on this oscillatory component.

To extract the low-frequency component, a moving average filter with a window size of 1000 was employed to avoid phase delay. Frequency analysis using the Fast Fourier Transform (FFT) was then performed on the residual signal obtained by removing the low-frequency component from the original signal, to evaluate oscillatory steering behavior.

The frequency analysis results for the first rider are shown in Fig. 8.The pink graph represents the analysis results without any items. Additionally, the results for trail lengths of 0.13 m, 0.085 m, and -0.035 m are shown in blue, green, and red, respectively. When the trail length is 0.13 m, vibration components increase in the range of 0–1.6 Hz, excluding 0.5 Hz and 1.0 Hz. In particular, increases are seen at 0.8 Hz and 0.9 Hz. When the trail length is 0.085 m, vibration components below 0.8 Hz are reduced. However, vibration components between 0.9 Hz and 1.4 Hz increase, particularly at 0.9 Hz and 1.0 Hz. When the trail length is -0.035 m, vibration components between 0.4 Hz and 0.7 Hz are reduced, while those between 0.9 Hz and 1.4 Hz increase. Although the frequency trends differ from those in the simulation, the results are consistent in showing reduced low-frequency and increased high-frequency components.

The frequency analysis results for the second rider are shown in Fig. 9. When the trail length is 0.13 m, vibration components increase in the range of 0–1.6 Hz, excluding 0.5 Hz and 0.9 Hz. In particular, increases are observed at 0.4 Hz and 0.6 Hz. When the trail length is 0.085 m, vibration components at 0.3 Hz and 0.5 Hz are reduced. However, vibration components between 0.4 Hz and 1.2 Hz increase, particularly at 1.2 Hz. When the trail length is -0.035 m, vibration components increase across the 0.4–1.7 Hz range. The second rider showed little reduction in vibration components, but an increase across a wide frequency range.

The frequency analysis results for the third rider are shown in Fig. 10. When the trail length is 0.13 m, vibration components increase within the range of 0.4–1.4

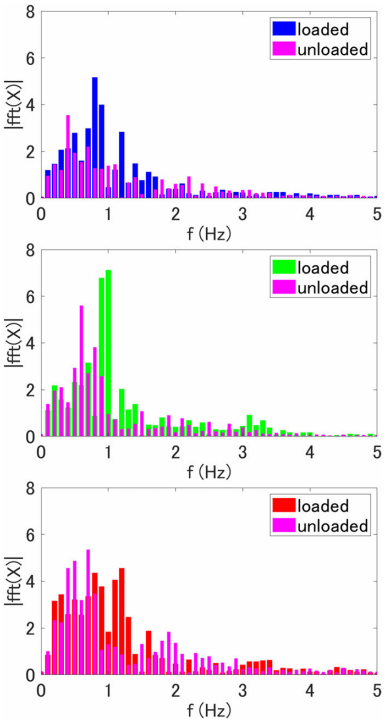

Fig. 8 FFT results for subject 1

Hz, excluding 0.5 Hz. When the trail length is 0.085 m, a noticeable reduction in components below 1.0 Hz is observed. However, vibration components between 1.2 Hz and 1.6 Hz increase. When the trail length is -0.035 m, reductions are seen between 0 and 0.8 Hz, excluding 0.4 Hz, while components between 0.9 Hz and 1.2 Hz increase. For the third rider, a reduction in vibration components was observed under conditions other than 0.13 m, along with a general increase in high-frequency vibra-

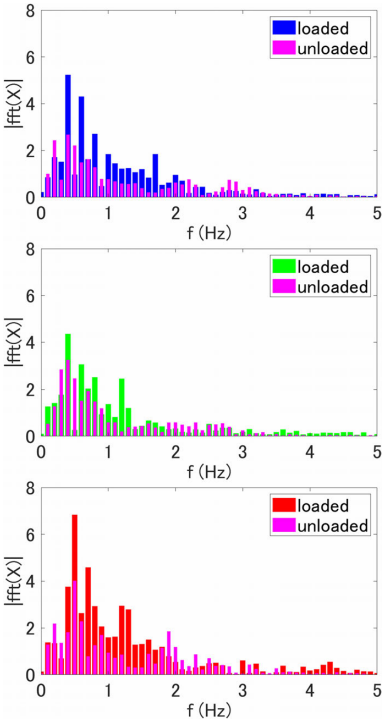

Fig. 9 FFT results for subject 2

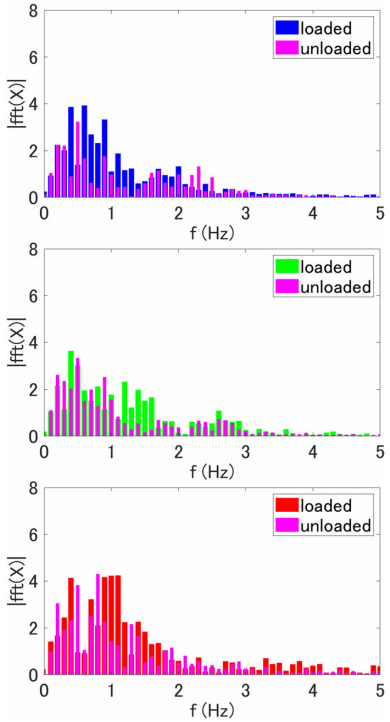

Fig. 10 FFT results for subject3

tion components.

A common result across all three riders was that placing a load on the rear of the bicycle induced oscillatory steering behavior. Simulation results further showed that the steering oscillations increased in frequency as the center of gravity shifted rearward. These findings suggest a relationship between rear loading and increased steering fluctuation.

5. CONCLUSION

In this study, as a preliminary step toward the development of a steering assist control law under rear-wheel loading conditions, the behavior of the bicycle during rear loading was analyzed. First, a mathematical model of the bicycle was derived for simulation-based behavioral analysis. Using this model, the changes in the riding behavior were evaluated under varying trail lengths and center of gravity positions. Next, to validate the simulation results, real-world riding experiments were conducted using an experimental bicycle equipped with a variable trail mechanism, with items loaded onto the rear carrier. By removing the steering components required for slalom riding from the measured steering angle data, unintended vibration components during riding were extracted.

The results clearly confirmed that rear carrier loading tends to induce oscillatory steering behavior, thereby achieving the intended behavioral analysis in this study. As future works, the mathematical model will be refined based on experimental data to enable more accurate behavioral reproduction. Additionally, the mechanisms behind steering vibration and its impact on vehicle stability will be investigated in detail, and the development of a steering assist control law applicable under the rear loading conditions will be further advanced.

6. ACKNOWLEDGMENT

This study was partially supported by JSPS KAKENHI Grant Number 24K01008.

REFERENCES

[1] Matsuzawa, S., Sato, N., Iwase, M., ”Control design of electrically-assisted steering systems for bicycles with child restraint seats.”, *2012 American Control Conference (ACC)*,pp.2749–2754,2012.

[2] Sankaran, G., Palomino, M.A., Knahl, M., Siestrup, G., ”Towards a System Dynamics Framework for Human-Machine Learning Decisions: A Case Study of New York Citi Bike.”, *MDPI Applied Sciences*,vol. 14, No. 22, 2024.

[3] Bian, L., Hu, Q., Zhang, X., Wu, X., Tan, M., ”Dynamic Investigations of Shared Bicycle Operators ’ Competition Based on Profit Maximization. ”, *MDPI Applied Sciences*,vol. 14, No. 20, 2024.

[4] Yoshida, K., Sato, K., Yamanaka, Y., ”Simple Degree-of-Freedom Modeling of the Random Fluctuation Arising in Human-Bicycle Balance.”, *MDPI Applied Sciences*, Vol. 9, No. 10 , 2019.

[5] Sharp, R. S., ”On the Stability and Control of the Bicycle.”, *ASME*,vol. 61, No. 6, pages.060803, 2008.

[6] Schwab, A.L., Kooijman, J.D.G; Meijaard, J.P., ”Some recent developments in bicycle dynamics and control.”, *Russian Academy of Sciences*,pp. 695–702, 2008.

[7] Hatano,R., Tani, T., Iwase,M., ”Stability analysis and autonomous stabilization control of a bicycle based on a three-dimensional detailed physical model”, *IECON 2016 - 42nd Annual Conference of the IEEE Industrial Electronics Society*, pp. 334–329, 2016.

[8] Kooijman, J.D.G., Meijaard, J.P., Papadopoulos, J.M., Ruina, A., Schwab, A.L., ”A Bicycle can be Self Stable without Gyroscopic or Caster Effects”, *Science*,vol. 332, No. 6027, pp. 339–342, 2011.

[9] Matsuzawa, S., Iwase, M., Sadahiro, T.,Hatakeyama, S. ”Motion analysis by experiment and simulation for riding bicycles with children”, *IEEE International Conference on Systems*, pp. 859–864 , 2009.

[10] Kowata, T., Sato, N., Iwase, M. ”M. Power steering system for electrically assisted bicycles riding with toddlers — Experimental implementation and verification”, *IEEE RSJ International Conference on Intelligent Robots and Systems*, pp.679–684 , 2013.

[11] Kihara, T., Sugasawa, Y., Kuriyama, K., Iwase, M. ”Steering Assist Control for Bicycles with Variable Trail Effect”, *MDPI Applied Sciences*, Vol. 15, No. 1 , 2024.

[12] Milan,P;Fook,F.Y.”Analyzing the impact of bicycle geometry and cargo loading on the rideability and safety of cargo bikes: An investigative study”, *Heliyon*, Vol. 10, No. 8 ,pages.e29524, 2024.

[13] K.J. Astrom, R.E. Klein, A. Lennartsson, “Bicycle dynamics and control: adapted bicycles for education and research”, *JIEEE Control Systems Magazine*, vol. 25, No. 4, pp. 26–47, 2005.

[14] Limebeer, D. J. N., and Sharma, A. ”Burst Oscillations in the Accelerating Bicycle”, *Journal of Applied Mechanics*, vol. 77, No. 6,pages.061012, 2010.